Journal Name

ARTICLE

Two-dimensional CoNi nanoparticles@S,N-doped carbon composites derived from S, N-containing Co/Ni MOFs for high performance supercapacitors

Received 00th January 20xx,
Accepted 00th January 20xx

DOI: 10.1039/x0xx00000x

www.rsc.org/

Mingyu Tong,‡[a,b] Shengwen Liu,‡[a] Xian Zhang,[a,b] Tianxing Wu,[a] Haimin Zhang,*[a] Guozhong Wang,[a] Yunxia Zhang,[a] Xiaoguang Zhu,[a] and Huijun Zhao*[a,c]

Owing to controllable morphologies, tunable porous structures, diverse compositions and easy to fabricate, metal organic frameworks (MOFs) have been a class of ideal precursor materials to develop high performance carbon-based materials for energy applications. In this work, two-dimensional (2D) Co/Ni MOFs nanosheets with a molar ratio of Co^{2+} to Ni^{2+} of 1:1 were first synthesized in room temperature using thiophene-2,5-dicarboxylate (Tdc) and 4,4´-bipyridine (4,4'-Bpy) as organic linkers. As precursor material, the as-synthesized 2D Co/Ni MOFs nanosheets were further pyrolized at 550 °C in N_2 atmosphere to obtain 2D CoNi alloy nanoparticles incorporated into S, N-doped carbon nanosheets (CoNi@SNC) with a surface area of 224 $m^2 g^{-1}$, porous structure, and good conductivity. Interestingly, it was found that 2D Co/Ni MOFs nanosheets can be directly used as electrode material for supercapacitor, delivering a specific capacitance of 312 F g^{-1} at 1 A g^{-1}, whereas CoNi@SNC derived from its MOFs precursor as electrode material for supercapacitor exhibits much higher specific capacitance (1970, 1897 and 1730 F g^{-1} at 1, 2, 5 A g^{-1}, respectively) with long cycling life (retaining 95.1% of the value at 10 A g^{-1} after 3000 cycles) and excellence rate capability at a high charge/discharge current. Further, an asymmetric supercapacitor device was also constructed with CoNi@SNC as the positive electrode and active carbon as the negative electrode, exhibiting an energy density of 55.7 Wh kg^{-1} at the power denstity of 0.8 kW kg^{-1} with lifetime stability up to 4000 charge-discharge cycles (capacitance retention of ~90.6%). The results demonstrate that electrochemical activation generated CoNi oxides/oxyhydroxides on the surface of CoNi alloy nanoparticles in alkaline electrolyte during electrochemical measurements should be the electrochemical active species of CoNi@SNC constructued supercapacitor. Besides of that, the high performance of CoNi@SNC constructed supercapacitor could be collectively due to its relatively high surface area favourbale for the exposure of electrochemical active sites, porous structure to promote redox-related mass transport, and CoNi alloy nanoparticles combined with graphitic carbon as electron collector to improve electron transfer.

Introduction

Supercapacitors, with fast recharging capability, high power density and long lifespan, are considered as ideal candidates for energy storage devices.[1-3] They can complement or replace traditional capacitors or batteries, especially when high power delivery or energy recycle is in need, which is crucial to meet the challenge of global warming and the finite fossil fuels.[1] The energy of supercapacitor is stored either by ions/electrons adsorption (electrical double layer capacitors) or fast redox reactions (pseudo-capacitors),[2] which is highly dependent on the properties of electrode materials such as electrochemical active sites, adjustable pore structure, enhanced conductivity as well as electrolyte-accessible surface areas *etc*.[4]

To date, high supercapacitor performance has been achieved through redox reactions aroused from a series of pseudo-capacitive nanomaterials,[2, 4] such as metal oxides,[5] metal hydroxides,[6-10] and polymers,[11] which have brought the energy density of electrochemical capacitors close to that of batteries.[2] Transition metal possessing multiple oxidation states is desirable for reversible redox reactions in pseudo capacitance generation. For example, RuO_2 has been widely studied as supercapacitor electrode material owing to its good conductivity and three distinct oxidation states delivering high capacitance,[12] but high cost and source scarcity limits its large-scale production application in supercapacitor. Comparatively, less expensive and abundant transition metal materials with multiple oxidation states, such as $Co(OH)_2$,[7] $Ni(OH)_2$,[8, 10] Co_3O_4,[12] NiO[5] and MnO_2,[13-16], $NiCo_2O_4$[17, 18] have been

[a] Key Laboratory of Materials Physics, Centre for Environmental and Energy Nanomaterials, Anhui Key Laboratory of Nanomaterials and Nanotechnology, CAS Center for Excellence in Nanoscience, Institute of Solid State Physics, Chinese Academy of Sciences, Hefei 230031, China.
E-mail: zhanghm@issp.ac.cn, h.zhao@griffith.edu.au
[b] University of Science and Technology of China, Hefei 230026, China
[c] Centre for Clean Environment and Energy, Griffith University, Gold Coast Campus, QLD 4222, Australia

† Electronic Supplementary Information (ESI) available: Supporting XRD patterns, TEM image, Raman Spectra and CV curves of the fabricated materials. See DOI: 10.1039/x0xx00000x

‡ These authors contributed equally to this work

extensively considered as an ideal substitution for supercapacitor applications. However, the shortcoming of these transition metal oxides/hydroxides as supercapacitor electrode materials is their poor conductivity and stability during measurements, leading to low supercapacitor performance. Recently, transition metal alloy materials such CoNi alloy nanoparticles have exhibited great potential as electrode materials for high performance supercapacitors in alkaline electrolyte.[19, 20] These reported studies demonstrated that CoNi alloy nanoparticles can not only provide more electrochemical active sites created by their oxides/oxyhydroxides generated on the surface of CoNi alloy nanoparticles through electrochemical activation in alkaline electrolyte, but also significantly improve electrode material's conductivity owing to the role of CoNi alloy particles as electron collector, thus improving the performance of supercapacitor.[16] A recent study on Ni-Co double hydroxides has discovered that Ni-rich active species ensure higher capacitance, while Co-rich species contribute better rate performance and long cycle life due to their higher electronic conductivity.[21] To further improve supercapacitor performance, development of CoNi alloy nanoparticles electrode materials with small particle size, high surface area, porous structure and superior conductivity is still highly desirable.

Incorporation of Co/Ni-based active components into porous carbon structures has been widely adopted to fabricate high performance electrode materials for supercapacitors.[18, 19, 22-25] The advantages of the above approach mentioned are: (1) the formed carbon material concurrently as reduction reagent to in situ reduce Co^{2+}/Ni^{2+} on carbon structure into metal Co or Ni or CoNi alloy nanoparticles; (2) carbon material with high surface area capable of improving the dispersibility of Co or Ni or CoNi alloy nanoparticles, favourable for the exposure of electrochemical active sites; (3) the formed Co or Ni or CoNi alloy nanoparticles on carbon substrate with enhanced electrical conductivity, favourable for electron transfer; (4) the composite with porous structure to improve redox-related mass transport during electrochemical measurement. These advantages of the fabricated composites collectively contribute high supercapacitor performance when used as electrode materials. In this respect, we recently reported ultrafine CoNi alloy nanoparticles incorporated into porous graphitic carbon structure using NaCl as porous structure template and glucose as carbon source by simple pyrolysis treatment, as electrode material exhibiting a specific capacitance of 1091 F g^{-1} at a current density of 1 A g^{-1}.[19] Yang and co-workers fabricated a hybrid architecture of nickel-cobalt sulphide nanoparticles anchored on graphene frameworks via a chemical adsorption and transformation process, achieving a specific capacitance of 1492 F g^{-1} at 1 A g^{-1}.[23] In recent years, metal-organic frameworks (MOFs) derived metal/carbon composites have displayed great potential as electrode materials for energy applications due to their controllable pore architecture, highly exposed active sites and well distributed metal phase on carbon structures.[9, 24] Especially, two-dimensional (2D) MOFs derived 2D carbon-based composites can effectively shorten electrolyte ions and electrons diffusion path distance, making them ideal for the surface dependent electrochemical reactions.[24] Zhang *et al.* recently reported $CoS_{1.097}$/N-doped carbon nanocomposites derived from 2D N-containing MOFs nanosheets with an additional S source by simple pyrolysis treatment, as electrode material demonstrating a specific capacitance of 360.1 F g^{-1} at a current density of 1.5 A g^{-1}.[24] Taking full advantage of the properties of MOFs' adjustable morphology, structure and composition, it is very feasible to develop 2D transition metal alloy nanoparticles *(e.g.*, CoNi) incorporated into porous carbon structure as high performance electrode material for supercapacitor.

Herein, we first utilized thiophene-2,5-dicarboxylate (Tdc) and 4,4′-bipyridine (4,4'-Bpy) as organic linkers in the presence of Co^{2+} and Ni^{2+} sources to controllably fabricate 2D S, N-containing Co/Ni MOFs nanosheets in room temperature. Further, 2D CoNi alloy nanoparticles@S, N-doped porous carbon (CoNi@SNC) composite was obtained by simple pyrolysis treatment of 2D S, N-containing Co/Ni MOFs nanosheets precursor in N_2 atmosphere. The as-prepared 2D Co/Ni MOFs and CoNi@SNC as electrode materials were evaluated for supercapacitor. The results demonstrated that the 2D Co/Ni MOFs constructed supercapacitor can deliver a specific capacitance of 312 F g^{-1} at a current density of 1 A g^{-1}, whereas the supercapacitor assembled with 2D Co/Ni MOFs derived CoNi@SNC exhibits much higher specific capacitance (1970, 1897 and 1730 F g^{-1} at 1, 2, 5 A g^{-1}, respectively) with long cycling life (retaining 95.1% of the value at 10 A g^{-1} after 3000 cycles) and excellent rate capability at a high charge/discharge current, comparable or superior to that of some reported Co/Ni-based carbon composite electrode materials (Table S1, ESI†). The high performance of CoNi@SNC constructed supercapacitor could be ascribed to more electrochemical active sites provided by CoNi nanoparticles on S, N-doped carbon nanosheets during electrochemical measurement, high surface area and porous structure of composite favourable for the exposure of electrochemical active sites and redox-related mass transport, and superior conductivity of composite to improve electron transfer. In this work, an asymmetric supercapacitor device was also constructed with CoNi@SNC as the positive electrode and active carbon as the negative electrode for further evaluation.

Experimental

Materials: Thiophene-2,5-dicarboxylate (Tdc, 98%, Aladdin Reagent), 4,4′-bipyridine (4,4'-Bpy, 98%, Aladdin Reagent), Acetylene black, polytetrafluoroethylene (PTFE), Nickel chloride ($NiCl_2{\cdot}6H_2O$), cobalt chloride ($CoCl_2{\cdot}6H_2O$), sodium hydroxide (NaOH) were all purchased and used without any further modification.

Synthesis of 2D Co/Ni MOFs nanosheets and 2D CoNi@SNC: The synthesis of 2D Co/Ni MOFs nanosheets was operated in room temperature. 296 mg 4,4'-Bpy, 280 mg Tdc and 132 mg NaOH were first dissolved in 20 mL of deionized water under ultrasound. Then,

5.0 mL of deionized water containing 114 mg $CoCl_2·6H_2O$ was added into the above mixed solution slowly. Subsequently, 30 mL of deionized water was added to the above mixture to get homogeneously dispersed outcomes. After 5 min under stirring, another 5 mL of deionized water containing 114 mg $NiCl_2·6H_2O$ was added into the aforementioned mixture. After 5 min, the product was filtered to collect, followed by washing using deionized water for 3 times. Finally, the obtained product was dried at 60 °C for overnight. For comparison, Co-MOFs or Ni-MOFs was also prepared by adding 228 mg $CoCl_2·6H_2O$ or $NiCl_2·6H_2O$ in reaction system through similar preparation procedure as Co/Ni MOFs nanosheets.

In a typical preparation procedure of 2D CoNi@SNC, the as-prepared 2D Co/Ni MOFs nanosheets were used as precursors for pyrolysis treatment at 550 °C for 2 h at a temperature raising rate of 5° min^{-1} in N_2 atmosphere to obtain 2D CoNi nanoparticles@S, N-doped carbon (2D CoNi@SNC) composites. Also, the as-prepared Co-MOFs and Ni-MOFs were utilized as precursors for pyrolysis treatment at 550 °C for 2 h in N_2 atmosphere to fabricate Co@SNC and Ni@SNC samples for comparison.

Characterizations: Morphological images of the samples were taken on a field emission scanning electron microscopy (FESEM, Quanta 200 FEG) operated at an accelerating voltage of 10.0 kV. To analyze the crystal phase of the samples, powder X-ray diffraction (XRD) patterns were recorded on a Philips X-Pert Pro X-ray diffractometer with Cu-Kα radiation (1.5418 Å). Transmission electron microscopy (TEM) and scanning transmission electron microscopy (STEM) images of the samples were recorded by a high resolution TEM (Philips TecnaiG2 F20), operated at an acceleration voltage of 200 kV. X-ray photoelectron spectroscopy (XPS) analysis was performed on an ESCALAB 250 X-ray photoelectron spectrometer (Thermo, America) equipped with A1 $K\alpha_{1,2}$ monochromatized radiation at 1486.6 eV X-ray source. The surface area and porosity of samples were measured by a Surface Area and Porosity Analyzer (Tristar 3020 M). Raman spectra of the samples were recorded on a LabRAM HR800 confocal microscope Raman system (Horiba Jobin Yvon) using an Ar ion laser operating at 532 nm. The content of cobalt and nickel in sample was determined through an inductively coupled plasma atomic emission spectrophotometer (ICP-OES, ICP-6300, Thermo Fisher Scientific, USA).

Electrochemical measurements: For electrochemical tests, the working electrode used for supercapacitor was prepared by mixing 80 wt.% CoNi@SNC composite, 15 wt.% acetylene black and 5.0 wt.% polytetrafluoroethylene (PTFE, 5.0 wt.% in water) binder. The resulting slurry was pressed on 1.0 cm × 1.0 cm nickel foam at 10.0 MPa. All electrochemical measurements were performed on a Zennium electrochemical workstation (Zahner) in a three-electrode cell configuration using Hg/HgO as the reference electrode and Pt plate as the counter electrode. The electrolyte was 6.0 M KOH solution. Cyclic voltammetry (CV) curves were recorded between -0.1 V and 0.6 V (*vs.* Hg/HgO) at various scan rates ranging from 5.0 to 50

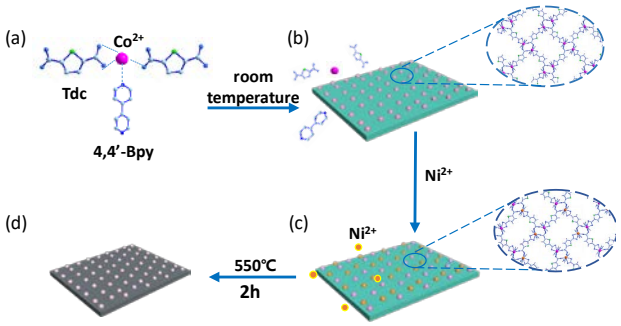

Fig. 1 Schematic illustration of the fabrication of 2D CoNi@SNC composites. (a) constitution unit; (b) Co-MOFs; (c) Co/Ni MOFs; (d) CoNi@SNC.

mV s^{-1}. Galvanostatic charge-discharge tests were conducted in the potential range of 0~0.5 V. For meaningful comparison, Co/Ni MOFs, Co@SNC and Ni@SNC were also used as electrode materials for supercapacitor measurements. Specific capacitance was calculated based on the active material using the following formula:

$$C = I\Delta t / (m\Delta V)$$

where I is the discharge current, Δt is the discharge time, m is the mass of the active electrode material, and ΔV is the voltage window. All electrochemical measurements were

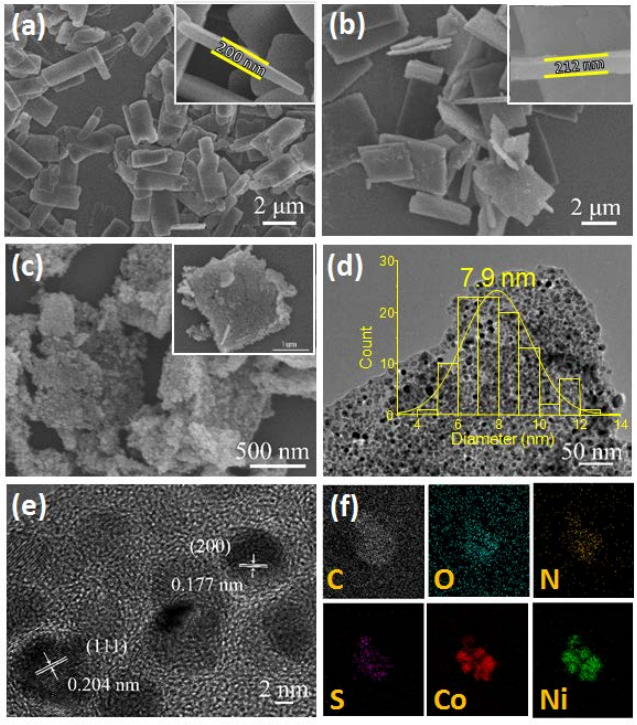

Fig. 2 Low magnified SEM images of (a) Co-MOFs; (b) Co/Ni MOFs; (c) CoNi @SNC; Top insets of magnified SEM images of the samples, respectively. (d) TEM image; Inset of statistical analysis of the CoNi particle sizes; (e) HRTEM image and (f) EDS mapping images of CoNi@SNC.

performed at room temperature. An asymmetric supercapacitor was fabricated with CoNi@SNC as the positive electrode, active carbon (AC) as the negative electrode, and a cellulose paper as the separator. Energy density (*E*) and power density (*P*) can be calculated as follows:

$$E = 0.5C\Delta V^2$$
$$P = E/\Delta t$$

where *C* is the specific capacitance, ΔV is the potential range between positive and negative electrodes, Δt is the discharging time, respectively. Electrochemical impedance spectrometry (EIS) was performed by CHI 660D electrochemical workstation at frequency ranging from 100 kHz to 10 mHz.

Results and discussion

In this study, utilizing Tdc and 4,4'-Bpy dual organic linkers in the presence of Co^{2+} and Ni^{2+}, $[CoNi(Tdc)(Bpy)]_n$ MOFs were synthesized in alkaline environment by a facile room-temperature solution reaction (Fig. 1). Alkaline reaction medium is beneficial for the deprotonation of Tdc, thus promoting the formation of 2D Co-Tdc rectangle-grid layers.[26, 27] Further, slightly dissolved Bpy in alkaline reaction solution at room temperature owing to its non-polar property links 2D Co-Tdc rectangle-grid layers into 2D Co-MOFs nanosheets with less Bpy pillar layers (Fig. 1).[26, 27] Further adding Ni^{2+} source into reaction system, $[CoNi(Tdc)(Bpy)]_n$ MOFs (Co/Ni MOFs) nanosheets were formed by a continuous growth of $[Ni(Tdc)(Bpy)]_n$ MOFs on the basis of $[Co(Tdc)(Bpy)]_n$ MOFs nanosheets (or possible a partial substitution of Ni^{2+} to Co^{2+} in MOFs structure) (Fig. 1). Besides of the role as organic linkers, Tdc and 4,4'-Bpy also provide S and N sources to form S, N-containing Co/Ni MOFs nanosheets during synthesis, favourable for creating more active sites for electrochemistry-related energy applications of MOFs derived carbon-based materials.[26, 27, 28]

Fig. 2a shows the SEM image of the as-prepared Co-MOFs in room temperature, and rectangular nanosheets with lateral sizes of ~2.0 μm and sheet thickness of *ca.* 200 nm can be clearly observed. After adding Ni^{2+} source into reaction system, the formed Co/Ni MOFs sample exhibits more flatly sheet-like morphology with larger nanosheet sizes and sheet thickness of *ca.* 212 nm (Fig. 2b and inset), indicating a continuous growth of Co-MOFs nanosheets after the introduction of Ni^{2+} source in the presence of Tdc and 4,4'-Bpy. The elemental mapping images of Co/Ni MOFs show that S, N, Co and Ni elements are uniformly distributed over the sample, possibly meaning the formation of Co/Ni MOFs (Fig. S1, ESI†). The ICP-OES analysis indicates that the molar ratio of Co to Ni in Co/Ni MOFs nanosheets is 0.98, close to 1:1. The XRD patterns demonstrate that the crystal phase of Co/Ni MOFs nanosheets can be indexed to an orthorhombic space group (*Pccn*), and the growth of (020) and (024) crystal planes is preferential, as shown in Fig. S2 (ESI†).[26] After pyrolysis treatment at 550 °C for 2 h in N_2 atmosphere, the as-prepared 2D Co/Ni MOFs nanosheets can be easily converted into carbon-based material with imperfect sheet-like structure and very rough surface (Fig. 2c). The morphologies of Co-MOFs and Ni-MOFs, and their corresponding pyrolysis products are shown in Fig. S3 (ESI†). As shown, Co-MOFs and Ni-MOFs all exhibit nanosheet

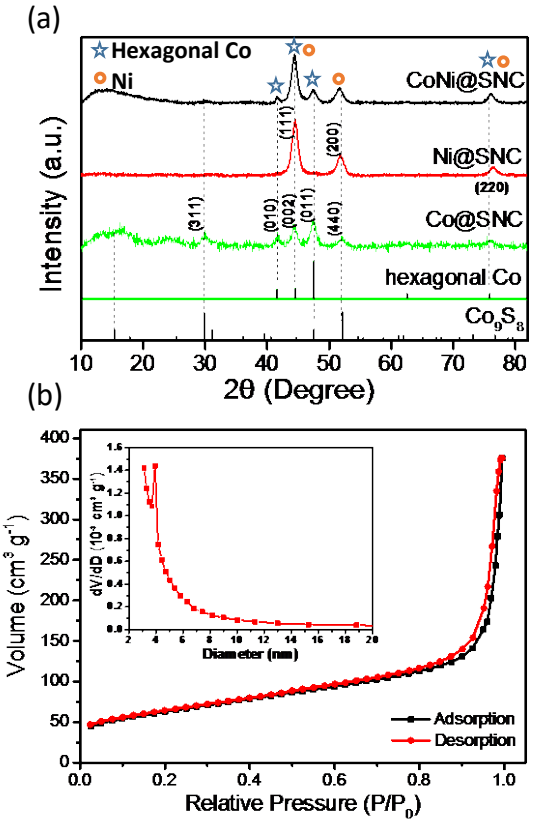

Fig. 3 (a) XRD patterns of Co@SNC, Ni@SNC and CoNi@SNC; (b) Nitrogen adsorption and desorption isotherm of CoNi@SNC; The inset shows the BJH pore size distribution curve.

structures, and after pyrolysis treatment, imperfect nanosheet structures with rough surface can be observed for their corresponding pyrolysis products. Many studies have demonstrated that the formed carbon structure during pyrolysis of MOFs precursor acts as dual role, namely, reduction reagent to reduce metal ions into active metal phase and conductive support for dispersed metal nanoparticles.[19, 22, 29] In this study, relatively uniformly dispersed nanoparticles with sizes of 5.0~15 nm can be clearly observed on carbon sheets after pyrolysis treatment of Co/Ni MOFs precursor, exhibiting an average particle size of ~7.9 nm (Fig. 2d). Further, the HRTEM image shown in Fig. 2e shows very clear crystalline planes with *d*-spacings of 0.204 nm and 0.177 nm, which can be ascribed to the (111) and (200) planes of metallic Co and Ni respectively, suggesting the formation of highly crystalline CoNi alloy nanoparticles on carbon sheet structure after pyrolysis treatment of Co/Ni MOFs nanosheets.[22, 30, 31] Fig. 2f shows the EDX mapping images of Co/Ni MOFs derived carbon material obtained from Fig. S4 (ESI†). As shown, Co/Ni MOFs derived carbon material is mainly composed of C, O, N, S, Co and Ni elements. It can be seen that N and S elements distribute relatively uniformly on the entire carbon structure, implying N, S doping in carbon structure. The uniform and overlapped distribution of Co and Ni elements located at nanoparticles further indicates the formation of CoNi alloy nanoparticles on carbon structure. Also, we found that the distribution of S element is more obvious located at CoNi nanoparticles, possibly meaning the formation of sectional Co or/and Ni sulfides during pyrolysis of Co/Ni MOFs. This could

be further confirmed by other characterization techniques. The above results demonstrate that after pyrolysis treatment, 2D Co/Ni MOFs nanosheets can be converted into 2D CoNi alloy nanoparticles@S, N-doped carbon (CoNi@SNC).

Fig. 3a shows the XRD patterns of carbon-based materials derived from Co/Ni MOFs, Co-MOFs and Ni-MOFs. As shown, Co-MOFs derived Co@SNC shows the diffraction peaks at 2θ=41.5, 44.5, 47.4°, corresponding hexagonal metallic Co phase (JCPDS card no. 96-900-8493, $Co_{2.00}$), while the diffraction peaks at 2θ=29.8, 47.5, 52.0° can be assigned to the (311), (511), (440) planes of cubic Co_9S_8 (JCPDS card no. 01-086-2273), indicating the co-existence of metallic Co and Co_9S_8 in Co@SNC. However, when the metal source is only Ni^{2+} in the process of MOFs synthesis, Ni-MOFs derived Ni@SNC exhibits only metallic Ni phase with diffraction peaks at 2θ=44.3, 51.6, 76.0°. For Co/Ni MOFs derived CoNi@SNC, the XRD patterns show the diffraction peaks at 2θ=44.3°, 51.67°, 76.10°, indexed to the (111), (200), (220) planes of CoNi alloy with atomic ratio approaching to 1:1.[22] The actually measured atomic ratio of Co to Ni is 0.89 (slightly lower than 1:1) in CoNi@SNC sample by ICP-OES, possibly meaning partial Ni^{2+} substituting Co^{2+} in MOFs structure. Except for the diffraction peaks of CoNi alloy, several weaker diffraction peaks at 2θ=29.8, 41.5, 47.4° can be ascribed to the (311) plane of cubic Co_9S_8 and (010), (011) planes of hexagonal Co, indicating a co-existence of Co_9S_8, hexagonal Co and CoNi alloy after pyrolysis of Co/Ni MOFs nanosheets. Although the intensity of Co_9S_8 is weaker compared to the strong diffraction peak of CoNi alloy, the Co_9S_8 component can be further confirmed by the line scanning images from STEM (Fig. S5, ESI†). This is in agreement with the elemental mapping results. Further, the sample was also characterized by the Raman spectra technique. In Fig. S6 (ESI†), the Raman spectrum of CoNi@SNC displays typical characteristic peaks of carbon materials at 1360 cm^{-1} of D-band and 1577cm^{-1} of G-band, respectively. They are often referred to as the vibrating of disorder graphite carbon atoms and in plane E_{2g} mode of graphite layer.[18, 32] Generally, the intensity ratio of G band to D band (I_G/I_D) is used to evaluate the degree of graphitization of carbon structure. The I_G/I_D ratio of CoNi@SNC is 1.04, indicating a graphitic carbon structure of the sample, favourable for improving the electrical conductivity of carbon material in electrochemical applications.[19, 29] It has been known that molten metals such as Ni, Co, Fe are highly effective in catalyzing the graphitization of carbon structures.[33] Amorphous carbons would be attacked by melted metals and recrystallize into more stable and well organized graphite.[34] Therefore, CoNi alloy particles are expected to have lower melting point than single metals facilitating the graphitization during carbonation.[35] The surface area and pore size distribution of 2D CoNi@SNC was measured by N_2 adsorption-desorption isotherms. As shown in Fig. 3b, the smooth hysteresis characteristic of the isotherm at high relative pressure (0.8-1.0) was observed, due to a typical type-III curve, indicating the existence of porous structure.[29, 36] Further, the surface area and pore volume of CoNi@SNC are 224 $m^2\ g^{-1}$ and 0.508 $cm^3\ g^{-1}$, respectively. The pore size distribution was calculated by the Barrett-Joyner-Halenda (BJH) method, as shown in the inset of Fig. 3b. A porous structure with two specific peaks centered at *ca.* 3.0 nm and 4.0 nm can be observed, indicating a primary mesoporous structure of CoNi@SNC. This mesoporous structure is very beneficial for improving the mass transport when CoNi@SNC is used as electrode material for electrochemical applications.

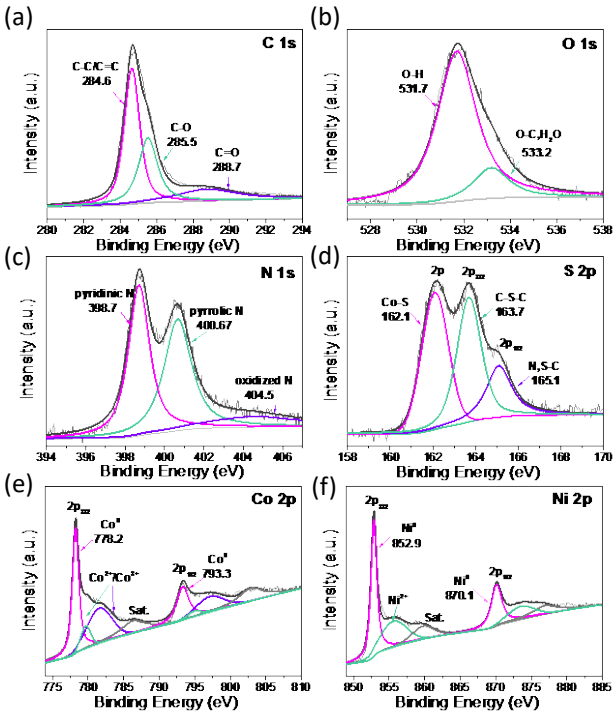

Fig. 4 High-resolution XPS spectra of (a) C 1s; (b) O 1s; (c) N 1s; (d) S 2p; (e) Co 2p and (f) Ni 2p of CoNi@SNC.

The surface elemental composition and chemical states of CoNi@SNC were analyzed by XPS technique and the results are displayed in Fig. 4. Consistent with the elemental mapping results, CoNi@SNC is consisted of C (70.28%), O(7.05%), N (7.52%), S (5.19%), Co(4.82%) and Ni(5.13%) elements. The high resolution C 1s XPS spectrum (Fig. 4a) can be fitted and divided into three peaks, corresponding to the aromatic-linked carbon (C=C, 284.6 eV), carbon-oxygen single bond (C-O, 285.5 eV) and carboxylate carbon (O-C=O, 288.7 eV).[18, 23] The existence of O element in CoNi@SNC could be mainly ascribed to the adsorption of H_2O molecules on the sample surface (Fig. 4b). In Fig. 4c, the high resolution N 1s spectrum can be deconvoluted to three sub-peaks, attributing to the pyridinic (398.7 eV), pyrrolic (400.67 eV) and oxidized N (404.5 eV), respectively, indicating N doping in Co/Ni MOFs converted carbon structure.[24] The high resolution S 2p XPS spectrum shown in Fig. 4d can be divided into three peaks at binding energies of 162.1 eV, 163.7 eV and 165.1 eV, corresponding to Co-S, C-S-C and S, N-C bonds, respectively.[18, 23, 27] The above results further confirm the formation of Co_9S_8 and S doping in carbon structure. As indicated in the Co 2p and Ni 2p XPS spectra (Fig. 4e, f), the main peaks were located at the binding energies of 778.2 eV and 793.3 eV (Fig. 4e), as well as the binding energies of 852.9 eV and 870.1 eV (Fig. 4f), indicating the existence of metallic Co and Ni in zero valent,[31, 37, 38] which is consistent with the XRD and TEM results of CoNi@SNC. Another two peaks at higher binding energies at Fig. 4e, f can be ascribed to metal oxides, possibly due to the partial oxidation of CoNi alloy nanoparticles.[23, 38] The remaining peaks of the Co and Ni 2p spectrum at 786.3 eV, 803.1 eV, 859.7 eV

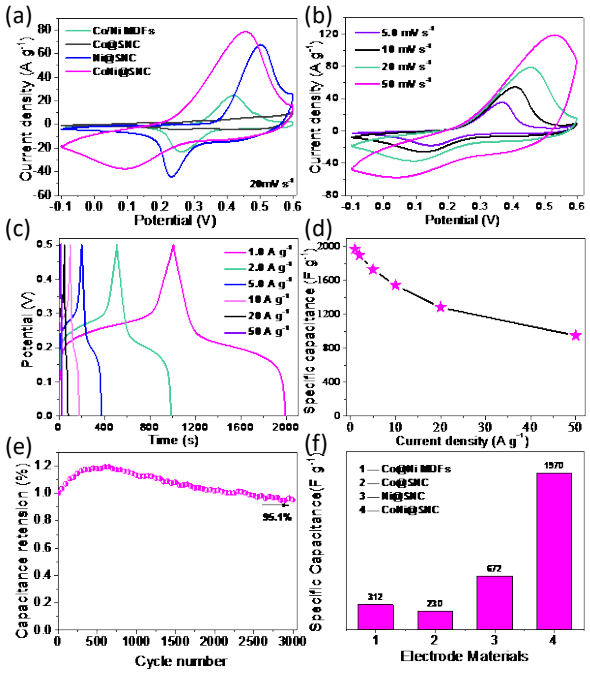

Fig. 5 (a) Cyclic voltammogram curves of different electrode materials; (b) CV curves at various scan rates; (c) Charge-discharge curves measured at different current densities; (d) Specific capacitance at various current densities, (e) Cycling performance at a constant current density of 10 A g^{-1} of CoNi@SNC; (f) Specific capacitance values of different electrode. materials measured at a current density of 1 A g^{-1}.

and 876.9 eV are deemed as shake-up satellites (denoted as "Sat.") due to plasmon losses and final state effects.[39-41] Combining with XRD and TEM analysis, the above XPS results further confirm the formation of primary CoNi alloy nanoparticles companying with partial Co_9S_8 in S, N-doping carbon structure derived from Co/Ni MOFs nanosheets precursor.

Electrochemical performance

Many studies have demonstrated that carbon-based materials with metallic Co or Ni or CoNi active species are very promising as high performance electrode materials for supercapacitors.[19, 42] Recently, some reported works have revealed that transition metal (*e.g.*, Fe, Co, Ni) organic frameworks are also potential electrode materials for supercapacitor applications through controllable growth of MOFs structures with the surface modification or the exposure of transition metal active sites as much as possible.[43-48] In this work, Co/Ni MOFs nanosheets and Co/Ni MOFs derived CoNi@SNC were used as electrode materials for supercapacitor evaluation. For meaningful comparison, Co-MOFs and Ni-MOFs derived Co@SNC and Ni@SNC were also used as electrode materials for measurements. First, the CV curves of Co/Ni MOFs nanosheets, CoNi@SNC, Co@SNC and Ni@SNC at a scan rate of 20 mV s^{-1} were measured in the potential window of -0.1~0.6 V (*vs.* Hg/HgO), as shown in Fig. 5(a). Compared to Co@SNC, Ni@SNC exhibits obvious redox peaks, implying the charge/discharge capability of Ni@SNC as supercapacitor electrode material. Comparatively, CoNi@SNC as electrode material shows broader redox peak area and larger redox peak intensity, promising for supercapacitor application. It has been generally accepted that the surface of CoNi alloy nanoparticles can be converted to Co_3O_4/NiO or $Co(OH)_2$/$Ni(OH)_2$ in alkaline solution for high supercapacitor performance.[19] Therefore, the cathodic peak at *ca.* 0.1 V and anodic peak at *ca.* 0.45 V at a scan rat of 20 mV s^{-1} may correspond to the fast and reversible electrochemical reactions of M-O/M-O-OH (M represents metal Co or Ni), primarily originated from the multiple variation of $Co^{2+}/Co^{3+}/Co^{4+}$ and Ni^{2+}/Ni^{3+} redox couples.[23, 49, 50] It should be noted that Co/Ni MOFs precursor as electrode material was found to be also electrochemically active with one pair of relatively small redox peaks, owing to Co/Ni-related active species in MOFs nanosheet structure.[45-47] Fig. 5b shows the representative CV curves of the electrode constructed by CoNi@SNC in the potential window of -0.1~0.6 V with various sweep rates ranging from 5.0 to 50 mV s^{-1}. According to these curves, a pair of broad redox peaks is visible in the CV curves, suggesting the pseudo-capacitive characteristics of CoNi@SNC electrode material. With the increase of sweep rate, the current density increases, and the position of anodic and cathodic peaks shifts toward a more positive and negative direction respectively, due to the polarization effect.[19] The well maintained CV shape implies that the electrode material could be applicable to the ultrafast redox reactions contributed supercapacitors.[19]

The galvanostatic charge/discharge measurements of CoNi@SNC electrode were carried out at different current densities (1.0~50 A g^{-1}) within a potential range of 0-0.5 V (*vs.* Hg/HgO). As shown in Fig. 5c, the curves at low current densities show two obvious platforms corresponding to the redox reactions resulted from Co/Ni active species. The potential-time curves at all current densities are near to be symmetric, indicating a high Coulombic efficiency due to the highly reversible redox reactions of CoNi@SNC electrode in the charge/discharge process.[23, 25] Fig. 5d describes the relation between specific capacitance and discharge current density. The CoNi@SNC exhibits 1970, 1897, 1730, 1543, 1282 F g^{-1} at the discharge current densities of 1.0, 2.0, 5.0, 10, 20 A g^{-1}, respectively, comparable or superior to that of some reported Co/Ni-based carbon composite electrodes (Table S1, ESI†). Apparently, specific capacitance decreases gradually with increasing current density, primarily due to the migration limitation of ions into the interior active sites of material, which is an indication of diffusion-controlled process.[4, 8] Long term cycling stability of electrode material is an important parameter of supercapacitor for practical application. Fig. 5e shows the repeated galvanostatic charge-discharge performance conducted at a constant current density of 10 A g^{-1} in 6.0 M KOH electrolyte. The specific capacitance of CoNi@SNC first increases until 600th cycle, and then slightly decreases, indicating a full activation of Co/Ni species in CoNi@SNC by effective contact between electrolyte and electrode materials required for high capacitor performance.[19, 51, 52] Compared with the first charge-discharge process, the specific capacitance of CoNi@SNC constructed supercapacitor exhibits ignorable decrease after 3000 cycles (about 95.1 % of capacitance can be retained), indicating high applicable stability of CoNi@SNC electrode. For comparison, the specific capacitance of Co/Ni MOFs, Co@SNC and Ni@SNC as electrode materials was also be measured to be 312, 230 and

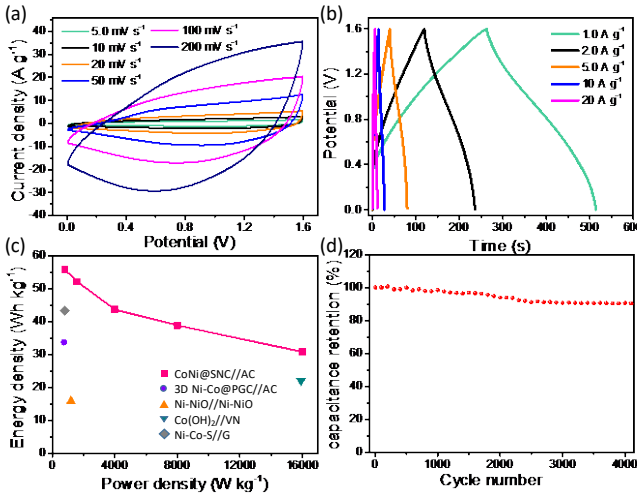

Fig. 6 Electrochemical performance of the CoNi@SNC//AC asymmetric supercapacitor. (a) CV curves at scan rates of 5.0-200 mV s^{-1}; (b) Galvanostatic charge-discharge curves at different current densities of 1-20 A g^{-1}; (c) The corresponding energy and power densities; and (d) Cycling performance at a constant current density of 10 A g^{-1}.

672 F g^{-1} at the discharge current density of 1.0 A g^{-1} in 6.0 M KOH electrolyte (Fig. 5f). Obviously, CoNi@SNC electrode exhibits much higher specific capacitance than that of Co/Ni MOFs, Co@SNC and Ni@SNC, possibly ascribed to several attributes of CoNi@SNC electrode material for supercapacitor: i) porous structure to improve mass transport, specific capacitance and rate capability, ii) high surface area favourable for the exposure of electrochemical active sites created by Co/Ni species (*e.g.*, oxides/oxyhydroxides), iii) high conductivity resulted from CoNi alloy nanoparticles combined with graphitic carbon to effectively improve electron transfer and ensure high rate capability. Collectively, these advantages of CoNi@SNC as electrode material contribute its high supercapacitor performance.

In order to investigate the practical application potential of CoNi@SNC for supercapacitor, an asymmetric device (CoNi@SNC//AC) was fabricated in 6.0 M KOH using CoNi@SNC as the positive electrode and active carbon (AC) as the negative electrode, with one piece of cellulose paper as the separator. The detailed electrochemical performance of AC electrode is presented in Fig. S7 (ESI†). Nearly rectangular shaped CV curves from -1.0 to 0 V can be observed for AC electrode, suggesting the double-layer nature capacitor. The voltage window was determined to be 1.6 V according to individual electrode behaviours. Fig. 6a shows the CV curves with scanning rates of 5.0 to 200 mV s^{-1}, and the nearly rectangular CV curves indicate the different supercapacitor activities in comparison with single CoNi@SNC or AC electrode. The charge-discharge curves of the asymmetric supercapacitor are shown in Fig. 6b. A high specific capacitance of 156.7 F g^{-1} can be reached at 1 A g^{-1} for the asymmetric supercapacitor, and the specific capacitance of 109.3 F g^{-1} at 10 A g^{-1}, delivering a 70% of capacitance retention. From the Ragone plot in Fig. 6c, it can be seen that the CoNi@SNC//AC asymmetric supercapacitor can afford a high energy density of 55.7 W h kg^{-1} at a power density of 0.8 kW kg^{-1}. These results

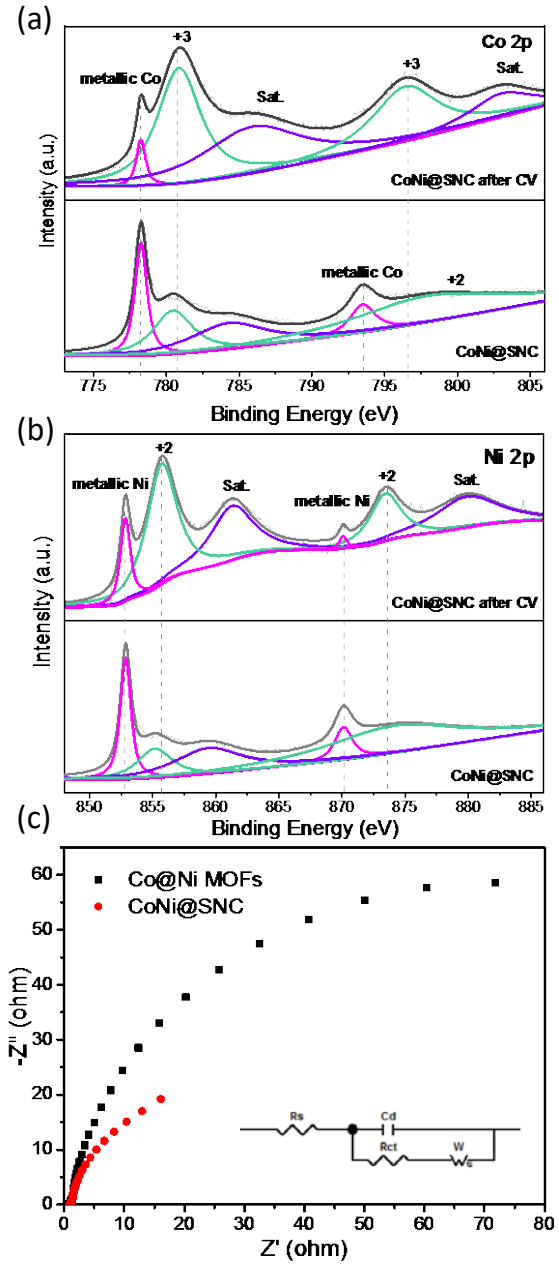

Fig. 7 XPS spectra of (a) Co 2p and (b) Ni 2p in CoNi@SNC before and after CV tests; (c) Nyquist plots of Co/Ni MOFs and CoNi@SNC.

are much better than those of 3D Ni-Co@PGC//AC (33.7 Wh kg^{-1} at 0.75 kW kg^{-1}),[19] Ni-NiO//Ni-NiO (15.9 Wh kg^{-1} at 0.12 kW kg^{-1}),[5] $Co(OH)_2$//VN (22 Wh kg^{-1} at 15.9 kW kg^{-1}),[7] Ni-Co-S//G(43.3 Wh kg^{-1} at 0.8 kW kg^{-1}).[23] In addition, the cycling performance of the asymmetric supercapacitor is measured at 10 A g^{-1} within the potential window of 0 - 1.6V for 4000 cycles, and the curves are displayed in Fig. 6d. The capacitance retention can reach 90.6% after 4000 cycles, indicating high stability of the asymmetric supercapacitor.

To further clarify the possible mechanism behind the charge-discharge process using CoNi@SNC as electrode material, CV curves from the 1th cycle to 1000th cycle were measured at a scan rate of 50 mV s^{-1} h, as shown in Fig. S8

(ESI†). It is obvious that the first CV cycle has shown a pair of redox peaks with a specific capacitance of 972 F g^{-1} at a current density of 2.0 A g^{-1}, possibly largely coming from the oxidation of the surface of CoNi alloy nanoparticles. Besides, the electrical double layer on the surface of S, N-doped carbon could also contribute the specific capacitance in a way.[29, 53] Teng and co-workers recently reported that the introduction of Ni species into carbon matrix can impart the carbon material with a surface polarity, thus enhancing dipole affinity towards OH^- and improving surface wettability of carbon material favourable for facilitating ion diffusion and increasing the ion-accessible surface area for high capacitance.[54] As shown in Fig. S8 (ESI†), with increasing cycling times, the current densities of redox peaks (especially for oxidation reaction) increase and tend to arriving a stable status after 600 cycles, further confirming the important role of a full activation of Co/Ni species in CoNi@SNC for high supercapacitor performance (the specific capacitance of 1660 F g^{-1} at a current density of 2.0 A g^{-1} after 1000 CV cycles). Further, we also performed the XRD characterization of CoNi@SNC after 1000 CV cycles to confirm the material component change before and after electrochemical measurement (Fig. S9, ESI†). Compared to the XRD patterns of CoNi@SNC, after electrochemical measurement, the diffraction peaks at 2θ=41.5 and 47.4° are almost disappeared and other diffraction peaks become weak, possibly meaning the formation of new component phase on the surface of CoNi alloy nanoparticles. However, no new diffraction peaks in XRD patterns of CoNi@SNC after electrochemical measurement can be clearly observed possibly due to a low content of the surface CoNi converted component phase. A well preserved morphology of CoNi@SNC after CV test can be observed by SEM technique, indicating its high applicable stability (Fig. S10, ESI†). Also, we conducted XPS analysis to further confirm the component change of CoNi@SNC after electrochemical measurement. As shown in Fig. 7a, b, strong metallic Co and Ni peaks can be observed in CoNi@SNC before 1000 CV measurements, while the peak intensities of metallic Co and Ni (peak positions at 778.2, 793.3, 852.9 and 870.1 eV) decrease and the peak intensities of Co^{2+}/Co^{3+} and Ni^{2+}/Ni^{3+} (peak positions at 781.6, 797.1, 855.6 and 873.5 eV) obviously increase, mainly owing to the surface CoNi alloy converted into corresponding oxides/oxyhydroxides resulting from the oxidation reaction during electrochemical test.[19] Briefly, at the earlier stage, CoNi alloy nanoparticles in CoNi@SNC undergo a reversible surface oxidation, which contributes some but relatively limited charge storage performance. After repeated charge and discharge process in alkaline environment, more active species (*e.g.*, Co/Ni oxides/oxyhydroxides) generate in the surface and interior of CoNi@SNC, resulting in high specific capacitance. Additionally, good conductivity of electrode material is critically important for its high capacitor performance. In this study, the electrochemical impedance spectroscopy (EIS) was achieved for Co/Ni MOFs and CoNi@SNC to investigate their performance as supercapacitor electrode materials, and an equivalent circuit used to fit the Nyquist plots, as shown in Fig. 7c and inset. Apparently, the almost same intercept on the real axis of these two electrode materials indicates a small internal resistance (R_s) of 0.71 Ω, which is composed of ionic resistance of electrolyte and the active material/current collector interface resistance.[6, 19] The diameter of semicircle of CoNi@SNC is much smaller than that obtained with Co/Ni MOFs, indicating that CoNi@SNC possesses lower charge transfer resistance (R_{ct}) and higher electrochemical activity owing to CoNi alloy nanoparticles providing more electrochemical reaction active sites.

Conclusion

In summary, CoNi alloy nanoparticles@S, N-doped carbon composite (CoNi@SNC) was successfully fabricated by a simple pyrolysis treatment of 2D S, N-containing Co/Ni MOFs nanosheets. Ascribed to high surface area, porous structure and superior electrical conductivity, CoNi@SNC as electrode material exhibited a specific capacitance of 1970 F g^{-1} at a current density of 1 A g^{-1} and excellent cycling stability with 95.1 % retention after 3000 cycles. The mechanism behind the high performance was explored to be the oxidation of metallic components to higher active species of oxides or hydroxides in alkaline environment. The findings in this work would be valuable for designing and developing transition metal alloy nanoparticles incorporated carbon electrode materials for high performance supercapacitors.

Acknowledgements

This work was financially supported by the National Natural Science Foundation of China (Grant No. 51372248, 51432009 and 51672277), the CAS Pioneer Hundred Talents Program and the CAS/SAFEA International Partnership Program for Creative Research Teams of Chinese Academy of Sciences, China.

Notes and references

1 J. R. Miller and P. Simon, *Science*, 2008, **321**, 651-652.
2 P. Simon and Y. Gogotsi, *Nat. Mater.*, 2008, **7**, 845-854.
3 D. P. Dubal, O. Ayyad, V. Ruiz and P. Gómez-Romero, *Chem. Soc. Rev.*, 2015, **44**, 1777-1790.
4 A. C. Forse, C. Merlet, J. M. Griffin and C. P. Grey, *J Am Chem Soc*, 2016, **138**, 5731-5744.
5 S. Ci, Z. Wen, Y. Qian, S. Mao, S. Cui and J. Chen, *Sci Rep*, 2015, **5**, 11919.
6 J. Xu, Y. Dong, J. Cao, B. Guo, W. Wang and Z. Chen, *Electrochimica Acta*, 2013, **114**, 76-82.
7 R. Wang, X. Yan, J. Lang, Z. Zheng and P. Zhang, *J. Mater. Chem. A*, 2014, **2**, 12724.
8 Y. Fu, J. Song, Y. Zhu and C. Cao, *Journal of Power Sources*, 2014, **262**, 344-348.
9 S. He, Z. Li, J. Wang, P. Wen, J. Gao, L. Ma, Z. Yang and S. Yang, *RSC Adv.*, 2016, **6**, 49478-49486.
10 Y. Zhu, C. Cao, S. Tao, W. Chu, Z. Wu and Y. Li, *Sci Rep*, 2014, **4**, 5787.
11 G. A. Snook, P. Kao and A. S. Best, *Journal of Power Sources*, 2011, **196**, 1-12.
12 S. K. Meher and G. R. Rao, *J. Phys. Chem. C*, 2011, **115**, 15646-15654.
13 H. Xia, Y. Shirley Meng, G. Yuan, C. Cui and L. Lu, *Nano Lett.*, 2011, **11**, 4438–4442.
14 S. Shi, C. Xu, C. Yang, Y. Chen, J. Liu and F. Kang, *Sci Rep*, 2013, **3**, 2598.

15 X. Xie, C. Zhang, M. B. Wu, Y. Tao, W. Lv and Q. H. Yang, *Chem. commun.*, 2013, **49**, 11092-11094.
16 H. Wang, Z. Lu, D. Qian, Y. Li and W. Zhang, *Nanotechnology*, 2007, **18**, 115616.
17 J. Hu, M. Li, F. Lv, M. Yang, P. Tao, Y. Tang, H. Liu and Z. Lu, *Journal of Power Sources*, 2015, **294**, 120-127.
18 D. Li, Y. Gong and C. Pan, *Sci Rep*, 2016, **6**, 29788.
19 S. Liu, Q. Zhao, M. Tong, X. Zhu, G. Wang, W. Cai, H. Zhang and H. Zhao, *J. Mater. Chem. A*, 2016, **4**, 17080-17086.
20 R. P. Silva, S. Eugenio, T. M. Silva, M. J. Carmezim and M. F. Montemor, *Corros. Prot. Mater.*, 2013, **32**, 37-41.
21 M. Yang, H. Cheng, Y. Gu, Z. Sun, J. Hu, L. Cao, F. Lv, M. Li, W. Wang, Z. Wang, S. Wu, H. Liu and Z. Lu, *Nano Research*, 2015, **8**, 2744-2754.
22 C. Jiao, L. Sun, F. Xu, S. S. Liu, J. Zhang, X. Jiang and L. Yang, *Sci Rep*, 2016, **6**, 27429.
23 J. Yang, C. Yu, X. Fan, S. Liang, S. Li, H. Huang, Z. Ling, C. Hao and J. Qiu, *Energy Environ. Sci.*, 2016, **9**, 1299-1307.
24 F. Cao, M. Zhao, Y. Yu, B. Chen, Y. Huang, J. Yang, X. Cao, Q. Lu, X. Zhang, Z. Zhang, C. Tan and H. Zhang, *J Am Chem Soc*, 2016, **138**, 6924-6927.
25 Y. Zhang, C. Sun, H. Su, W. Huang and X. Dong, *Nanoscale*, 2015, **7**, 3155-3163.
26 H.-P. Jia, W. Li, Z.-F. Ju and J. Zhang, *Eur. J. Inorg. Chem.*, 2006, **2006**, 4264-4270.
27 X. Zhang, S. Liu, Y. Zang, R. Liu, G. Liu, G. Wang, Y. Zhang, H. Zhang and H. Zhao, *Nano Energy*, 2016, **30**, 93-102.
28 S. Liu, M. Tong, G. Liu, X. Zhang, Z. Wang, G. Wang, W. Cai, H. Zhang and H. Zhao, *Inorg. Chem. Front.*, 2017, **4**, 491-498.
29 W. Bao, A. K. Mondal, J. Xu, C. Wang, D. Su and G. Wang, *Journal of Power Sources*, 2016, **325**, 286-291.
30 X.-W. Wei, X.-M. Zhou, K.-L. Wu and Y. Chen, *CrystEngComm*, 2011, **13**, 1328-1332.
31 S. Zhou, M. Wen, N. Wang, Q. Wu, Q. Wu and L. Cheng, *J. Mater. Chem.*, 2012, **22**, 16858-16864.
32 P. Zhang, F. Sun, Z. Xiang, Z. Shen, J. Yun and D. Cao, *Energy Environ. Sci.*, 2014, **7**, 442-450.
33 W. Weisweiler, N. Subramanian and B. Terwiesch, *Carbon*, 1971, **9**, 755-761.
34 S.-S. Tzeng, *Carbon*, 2006, **44**, 1986-1993.
35 A. Tanaka, S.-H. Yoon and I. Mochida, *Carbon*, 2004, **42**, 591-597.
36 C. Zheng, C. Cao, Z. Ali and J. Hou, *J. Mater. Chem. A*, 2014, **2**, 16467-16473.
37 S. K. Singh, A. K. Singh, K. Aranishi and Q. Xu, *J Am Chem Soc*, 2011, **133**, 19638-19641.
38 G. Zhang, S. Sun, M. Bostetter, S. Poulin and E. Sacher, *J Colloid Interface Sci*, 2010, **350**, 16-21.
39 J. Pu, F. Cui, S. Chu, T. Wang, E. Sheng and Z. Wang, *ACS Sustainable Chem. Eng.*, 2014, **2**, 809-815.
40 V. H. Nguyen, C. Lamiel and J.-J. Shim, *Electrochimica Acta*, 2015, **161**, 351-357.
41 N.S. McIntyre and M.G. Cook, *Anal. Chem.* , 1975, **47**, 2208-2213.
42 A. G. El-Deen, M. El-Newehy, C. S. Kim and N. A. Barakat, *Nanoscale research letters*, 2015, **10**, 104.
43 J. Yang, C. Zheng, P. Xiong, Y. Li and M. Wei, *J. Mater. Chem. A*, 2014, **2**, 19005-19010.
44 L. Wang, X. Feng, L. Ren, Q. Piao, J. Zhong, Y. Wang, H. Li, Y. Chen and B. Wang, *J Am Chem Soc*, 2015, **137**, 4920-4923.
45 P. Wen, P. Gong, J. Sun, J. Wang and S. Yang, *J. Mater. Chem. A*, 2015, **3**, 13874-13883.
46 H. G. Ranjbar, M. Soleimani and H. R. Nader, *New J. Chem.*, 2016, **40**, 9187-9193.
47 Y. Jiao, J. Pei, C. Yan, D. Chen, Y. Hu and G. Chen, *J. Mater. Chem. A*, 2016, **4**, 13344-13351.
48 D. Sheberla, J. C. Bachman, J. S. Elias, C. J. Sun, Y. Shao-Horn and M. Dinca, *Nature materials*, 2016, DOI: 10.1038/nmat4766.
49 H. Wan, J. Jiang, J. Yu, K. Xu, L. Miao, L. Zhang, H. Chen and Y. Ruan, *CrystEngComm*, 2013, **15**, 7649.
50 W. Kong, C. Lu, W. Zhang, J. Pu and Z. Wang, *J. Mater. Chem. A*, 2015, **3**, 12452-12460.
51. W. Zeng, G. Zhang, X. Wu, K. Zhang, H. Zhang, S. Hou, C. Li, T. Wang and H. Duan, *J. Mater. Chem. A*, 2015, **3**, 24033-24040.
52. M. Jana, S. Saha, P. Samanta, N. C. Murmu, N. H. Kim, T. Kuila and J. H. Lee, *J. Mater. Chem. A*, 2016, **4**, 2188-2197.
53 L. Li, Z. Dai, Y. Zhang, J. Yang, W. Huang and X. Dong, *RSC Adv.*, 2015, **5**, 83408-83414.
54 Y.-L. Tai and H. Teng, *Carbon*, 2004, **42**, 2335-2338.